Tiling Efflorescence of Expanding Kernels in a Fixed Periodic Array: Generalizing the Flower-Of-Life

Robert J. Marks II

DOI: 10.33014/issn.2640-5652.3.1.marks.1

Abstract

Continually expanding periodically translated *kernels* on the two dimensional grid can yield interesting, beautiful and even familiar patterns. For example, expanding circular pillbox shaped kernels on a hexagonal grid, adding when there is overlap, yields patterns including maximally packed circles and a triquetra-type three petal structure used to represent the trinity in Christianity. Continued expansion yields the flower-of-life used extensively in art and architecture. Additional expansion yields an even more interesting emerging efflorescence of periodic functions. Example images are given for the case of circular pillbox and circular cone shaped kernels. Using Fourier analysis, fundamental properties of these patterns are analyzed. As a function of expansion, some effloresced functions asymptotically approach fixed points or limit cycles. Most interesting is the case where the efflorescence never repeats. Video links are provided for viewing efflorescence in real time.

Keywords: *tiling, emergence, periodicity, flower-of-life, efflorescence, triquetra*

1 Introduction

Expanding kernels on a periodic array can generate beautiful and sometimes familiar patterns.

To visualize how an expanding circular kernel might physically occur, imagine point sources of light that emit perfectly circular cones that expand with distance. This is illustrated in Figure 1. Assume a large number of these light sources are spaced in a hexagonal grid. A viewing screen placed parallel and close to the array of lights will display a set of circles as in Figure 2(a) because the cones have not yet overlapped. There will be a point where the cones first touch. This is illustrated in Figure 1 where a single hexagon of seven point elements sources are denoted by the small circles on top. The touching cones here correspond to the closely spaced nonoverlapping circles in Figure 2(b) and the maximally packed pennies in Figure 4. Beyond this point, the circles intersect. This visualization illustrates the dynamics in Figure 2 where the number of periodically spaced light sources on the plane is infinite. The further we go from the lights, the more circles overlap and the more interesting and beautiful patterns emerge.[1]

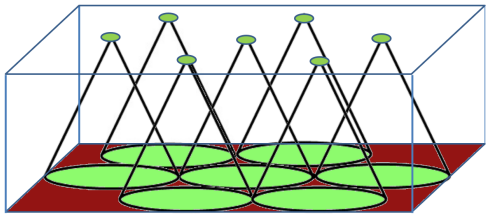

Figure 1: Illustration of the expanding kernels shown in Figure 2. Light sources give forth cone-shaped beams which overlap more and more as the distance is increased from the light source plane. Shown here is the point where the cones first touch. This corresponds to the circles in Figure 2(b).

From a first order approximation, expanding circles emerge from single x-rays in cone-beam tomography (Feldkamp, Davis, and Kress, 1984; Scarfe, 2018) generate the expanding circles in Figure 1. Expanding patterns other than cones naturally occur in electromagnetics. Periodically spaced antenna (Filipovic, Volakis, and Andersen, 1999; Ishimaru et al., 1985; Markov and Chaplin, 1983) and sensor arrays (Goussetis, Feresidis, and Vardaxoglou, 2006; Sung et al., 2008) generating identical expanding signals can display diverse and complex patterns depending on source excitation and range of observation.

The *tile* in this expanding circle example is a equalsided hexagons as used by bees in honey combs. The hexagonal tile for maximally packed circles is shown in Figure 5 where identical hexagonal tiles each containing an inscribed circle. Rectangles and parallelograms are other examples of possible

[1] As the cone expands, the light will grow dimmer. The analogy breaks down here. We assume the light in the plane always correspond to a brightness value of one no matter how far we are from the point sources.

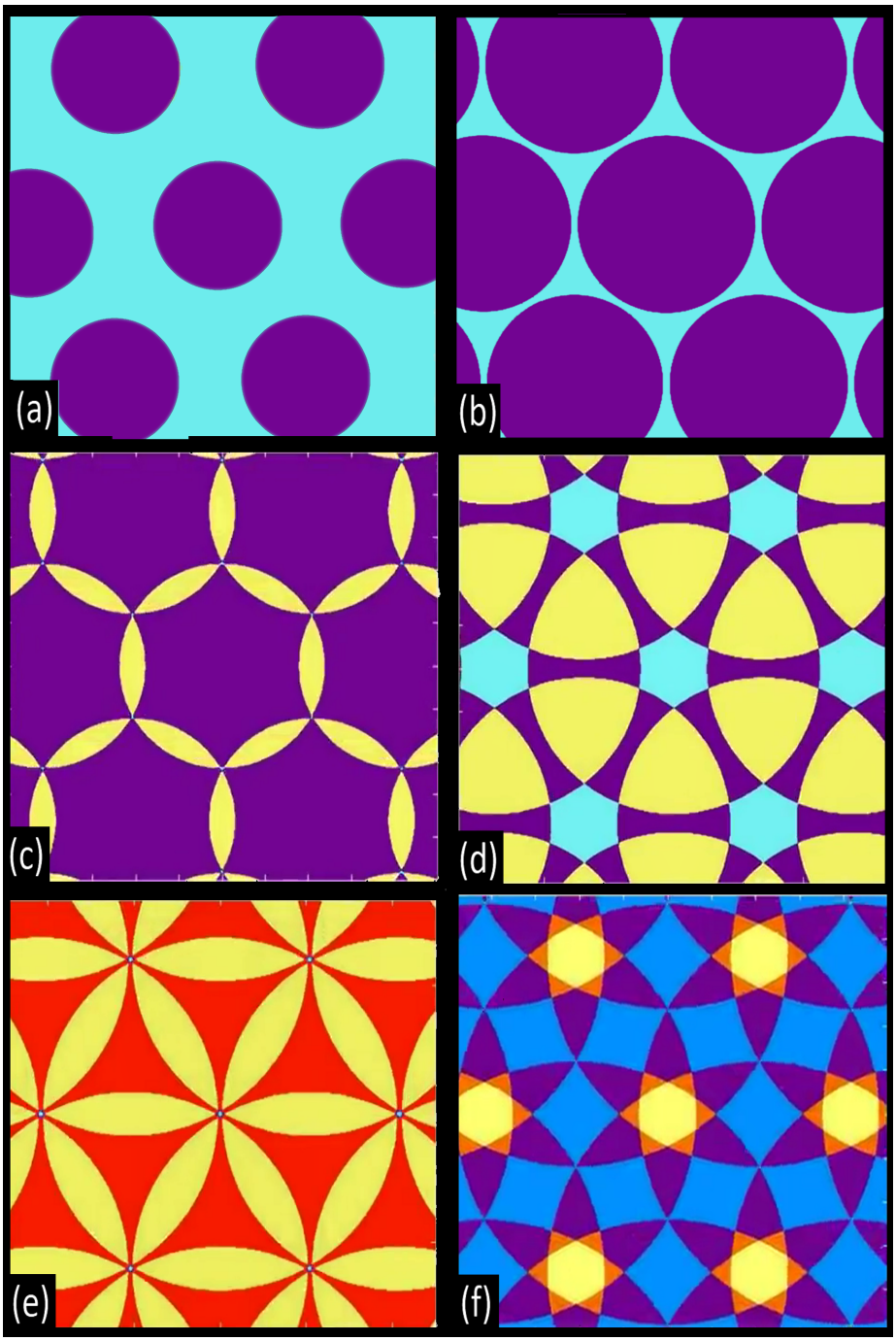

Figure 2: Expanding circular pillboxes on a hexagonal grid. Heat map (Wikipedia, 2020a) colours denote regions equal to a constant and are used only for differentiating among the different regions of the figure. Figure (b) represents maximally packed circles. Figure (c) is a three petal pattern. Slightly more expansion will result in the triquetra in Figure 7. Figure (e) is the flower-of-life. (Continued in Figure 3.)

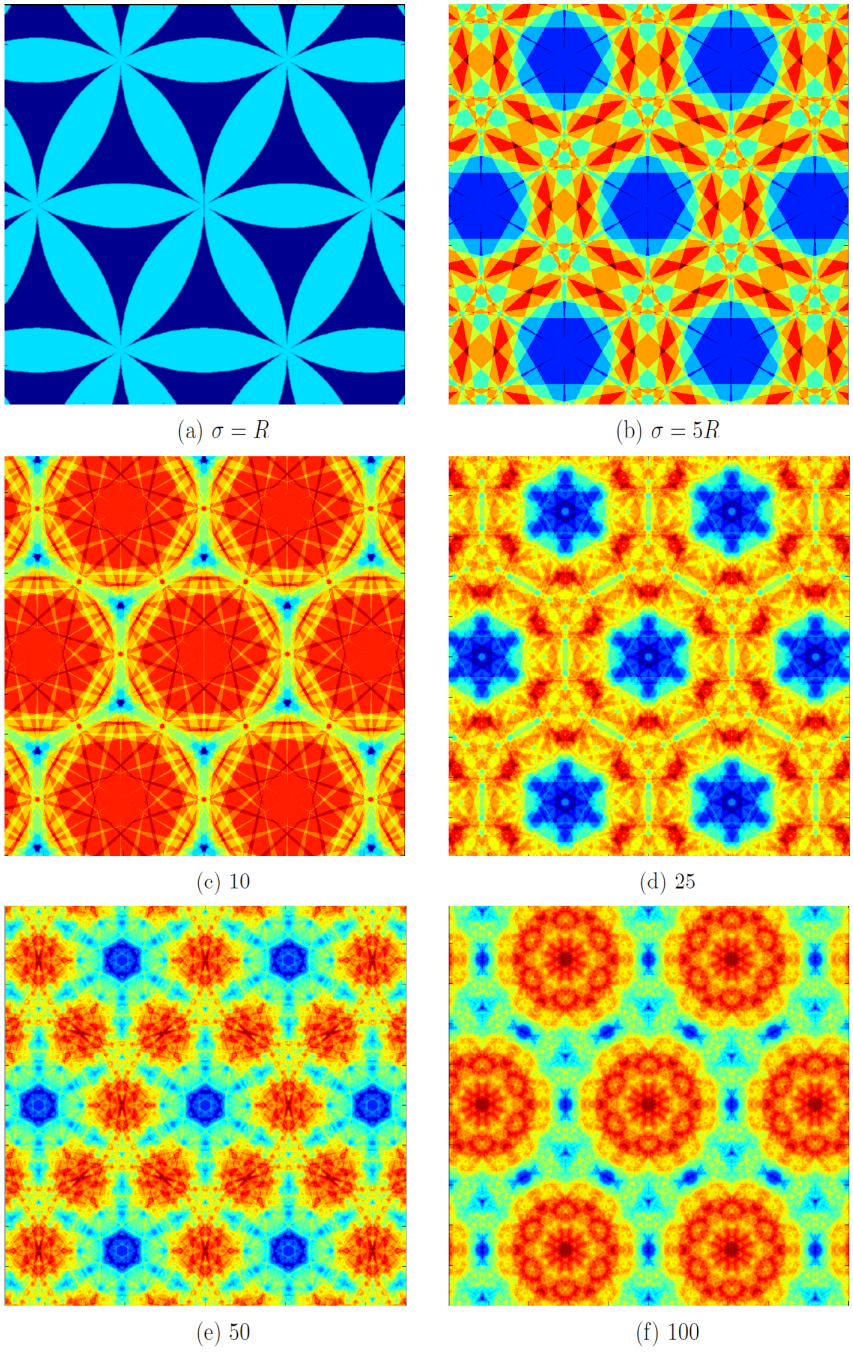

(a) $\sigma = R$ (b) $\sigma = 5R$

(c) 10 (d) 25

(e) 50 (f) 100

Figure 3: Heat map plots of expanding circular pillbox efflorescent function beyond that in Figure 2. As the circles expand, the patterns have more texture because higher and higher spatial frequencies are introduced. (Continued from Figure 2.)

Figure 4: Maximally packed pennies (Wikipedia, 2020b). In this example, the kernel is the grey level map of a single penny and the periodicity is hexagonal.

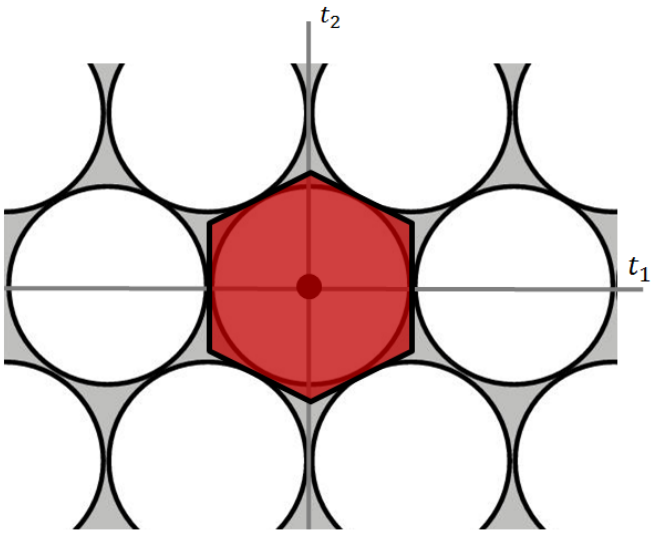

Figure 5: Maximally packed circles and the corresponding hexagonal tile.

tile shapes. Circles and octagons are not tiles since any tiling attempts will result in gaps of coverage.[2]

All the patterns in Figure 2 can be achieved with identically shaped hexagon tiles containing an appropriate pattern.

More generally, identical versions of a two dimensional (2D) function[3] are translated in accordance to a 2D periodic geometry specified by the two periodicity vectors. The translations are added to form a periodic function. We call the original 2D function the *kernel*. With the tiling geometry kept constant, each of these kernels is magnified or, equivalently, *expanded*. The expanding kernels will soon overlap onto other tiles. When kernels overlap, the expanded kernels are added. When viewing the emergent patterns as expansion continues, fascinating patterns can begin to flower. Since *efflorescence* in French means "to flower out," we refer to the emergence as *efflorescent functions*. No matter how much the kernels expand, the efflorescent function is a periodic function with a period fixed by the tile.

An alternate explanation of expanding kernels is illustrated in Figure 1 where the circular kernel is illustrated as an expanding circular pill box.

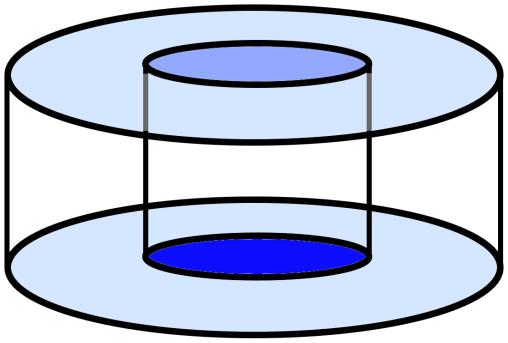

Figure 6: An expanding circular pillbox as a 2D function. The circular pillbox shape expands to the larger pillbox is a smooth continuous manner.

Independent of the degree of kernel expansion, the resulting

[2]Triangles are not considered tiles in our treatment. Two identical triangles can be be configured into a parallelogram tile, but we we only consider tiling that uses translation. No rotation or flipping is allowed. Nevertheless, rotation and flipping of so-called *subtiles* can be used in definition multidimensional periodicity (Marks II, 2019). This is not considered in our treatment.

[3]i.e. a scalar function of two variables.

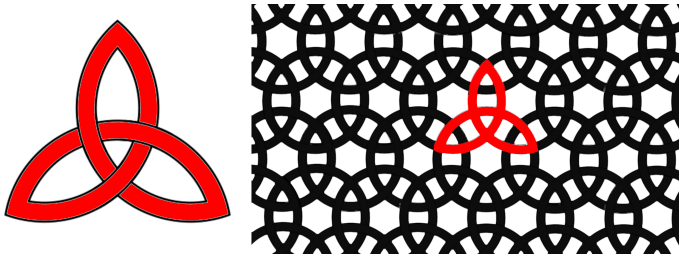

Figure 7: An illustration of a specific instance of expanded overlapping when the kernel is an annulus (circular ring) replicated hexagonally. Left: The triquetra (Wikipedia, 2020c). Right: Periodic replication of the triquetra reveals emergence from overlapping rings. (Note: The summation of the overlaps is not shown. Only the ring overlap is shown.)

2D function formed by the sum of possibly overlapping kernels is periodic with the same hexagonal replication geometry. The single hexagonal tile shown in Figure 5can be copied and, if you will, used to tile a kitchen floor without gaps. In this sense, a periodic tiling geometry is conserved during the expansion.[4]

Expanding circles generate familiar flowering instances including:

- packed circles in Figure 2(b) can be visualized by placing pennies on a table surface as close as possible. This is illustrated in Figure 4,
- as seen in Figure 7, a triquetra-type (Wikipedia, 2020c) three petal pattern used to represent the trinity in early Christianity. This pattern is seen in Figure 2(c), and
- the flower-of-life (Melchizedek, 1999) in Figure 2(e)[5]

Properties of efflorescent functions can be derived using two dimensional Fourier series analysis. Some efflorescent functions approach fixed points or limit cycles as a function of expansion. Most interesting are efflorescent functions that never repeat. Describing mathematics is limited to Section 4 and the Appendix. The content of the paper is thereby accessible without reference to the detail sought by mathematicians for deeper insight.

[4]For a given replication, there is more than one choice for a tile. Hexagonal tiles can be used for any of the patterns shown in Figure 2 but a parallelogram tile can be used to represent the same periodicity structure. Although tiles can differ geometrically, all viable tiles will have the same two-dimensional area (Marks II, 2009).

[5]The flower-of-life is easily constructed using only a compass. Draw a circle. Then place the point of the compass at any point on the circle. Draw another circle. Place the compass point at one of the two points where the circles intersect and draw another circle with the same radius. Continue placing the compass point at intersections of circles with the original circle and the flower-of-life will result.

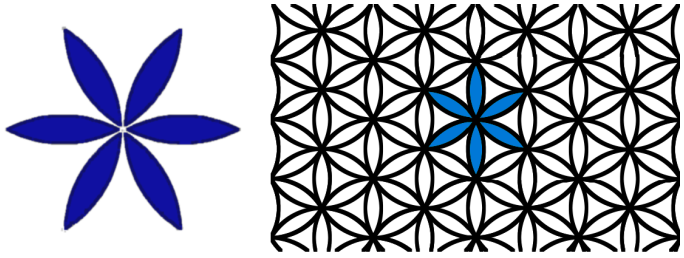

Figure 8: Left: The flower-of-life. Right: Periodic replication of the flower-of-life reveals emergence from overlapping circles.

1.1 The Flower-of-Life in Art History

The flower-of-life tiling has a rich history in art and architecture. The flower-of-life appears in the Osiris Temple in ancient Egypt (Flowers, 2006) and as a floor decoration from the palace of King Ashurbanipal. Ashurbanipal was king of the Neo-Assyrian Empire from 668 BC to c. 627 BC (Manninen, 2011). The flower-of-life even appears in crop circles (National Geographic, 2010) .

Here are some other examples.

1. As shown in Figure 10, the flower-of-life appeared in the art of Leonardo da Vinci (Mic, 2012).
2. Figure 10 shows the flower-of-life from Turkey.
3. In Figure 11, we see a cup fragment from Idalion, Cyprus that dates to circa 700 to 600 BC. The art shows "mythological scenes, a sphinx frieze and the representation of a king vanquishing his enemies. The center contains a version of the 'Flower of life' geometrical pattern" (Nguyen, 2007).
4. A ball "held by the male Imperial Guardian Lion at the Gate of Supreme Harmony, Forbidden City, Beijing. China" is covered by replications of the flower-of-life. This is shown in Figure 12.

1.2 Further Circle Expansion

What happens when the circles are expanded further than shown in Figure 2? Results is shown in Figure 3 starting with the flower-of-life in the upper left. Assume the original radius of the circles in the flower-of-life is $R = 1$. Shown are hexagonal tilings corresponding to the circle radiuses of 5, 10, 25, 50 and 100.

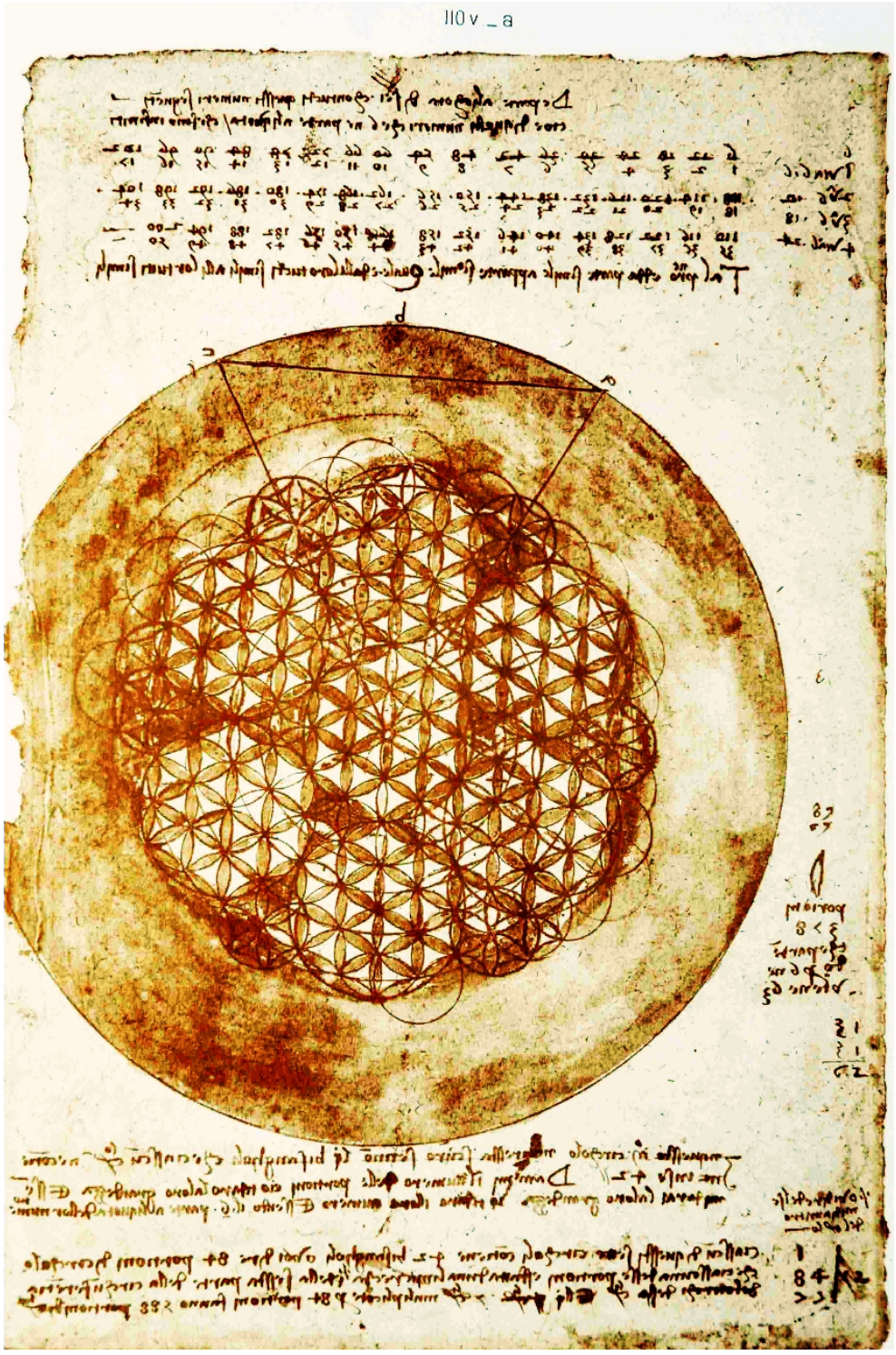

Figure 9: Flower of life from sketches from Leonardo da Vinci. (This is a faithful photographic reproduction of a two-dimensional, public domain work of art (da Vinci, 1478).)

Figure 10: Flower of life "ephesos square" from Ephesus, Turkey. (Image credit: Wikipedia Creative Commons Attribution-Share Alike 4.0 International (Miryam, 2015).)

Figure 11: An ancient cup inscibed with the flower-of-life. (Image credit: This work is in the public domain in its country of origin and other countries and areas where the copyright term is the author's life plus 100 years or fewer (Nguyen, 2007).)

Figure 12: The flower-of-life is on a ball at the Gate of Supreme Harmony, Forbidden City, Beijing. China. (Photo credit: Wikimedia Commons (Adamantios, 2013).)

Videos of beautiful emergent behavior from real-time expanding circular kernels are available online (Nybal, 2014d; Nybal, 2014c).

2 Other Expanding Kernels

Other kernels can be expanded and arrays other than hexagonal can be used. An expanding circular cone kernel[6] is illustrated in Figure 13. (Compare to the expanding pillbox circle in Figure 6.) A heat map plot of a hexagonal array of small nonoverlapping circular cones is shown in Figure 14(a). The overlapping expanding kernels are then shown for circle radii of $200, 500, 1000, 1500$, and 1750. As is the case with the circles, the patterns generally become more complex as the expansion becomes larger and more and more cones intersect.

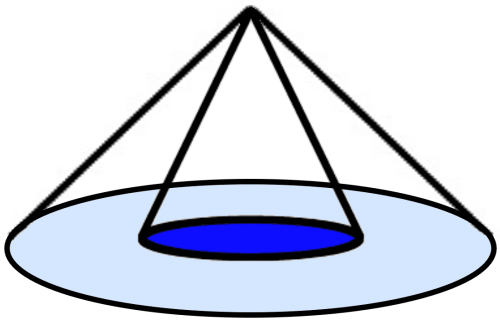

Figure 13: A single expanding circular cone shaped kernel as a two dimensional function.

3 Properties of Expanding Kernels of Varying Periodicity

3.1 Detrending and Heat Maps

As more and more kernels overlap, the number of kernels intersecting a tile generally gets larger and larger.[7] If 1000 circular pillboxes overlap and the height of a pillbox is one, the value of the 2D function is 1000 in the area of overlap. Detrending clears this tower by removing the buildup and looking only at fluctuations on top of the tower after removing the tower height.

In Fourier series, the zeroth order Fourier series coefficient denotes the average value of the periodic function. By setting the zeroth order coefficient to zero, the tower is removed and only the fluctuations remain. We define setting the zeroth order Fourier series coefficient to zero as *detrending* (Hill and Gauch, 1980; Kantelhardt et al., 2002). The heat map plots in Figures 2,3,14 and 15 do this automatically by plotting only within the dynamic range of the fluctuations.

3.2 Summary of Fourier Analysis Results

Depending on the kernel and periodicity, display of detrended patterns show different behaviour. In Section 4, we examine whether continuous expansion of kernels asymptotically approaches either:

1. zero everywhere,
2. a fixed periodic function of the $\vec{t}$ plane that does not change with respect to additional expansion, or
3. oscillation in a limit cycle as function of the expansion variable. In other words, as expansion continues, the efflorescent function displays a repeated pattern.

As we go down the list, each entry is seen to be a subset of the other. A value of (1) zero is a degenerate case of (2) a fixed periodic function that does not change with expansion. Likewise (2), a fixed periodic function, is a special static case of (3): oscillation on a limit cycle as a function of expansion.

The most interesting cases, not on the list, are those where the efflorescent function never repeats and results in a never repeating series of patterns. The expanding circular pillbox and circular cone are examples.

4 Analysis

The mathematical analysis of efflorescent functions is solely relegated to this section and the Appendix.

Using standard notation (Dudgeon and Mersereau, 1984; Marks II, 1991; Marks II, 2009), the two dimensional Fourier transform of a two dimensional function $x(\vec{t}) = x(t_1, t_2)$ is[8]

$$X(\vec{u}) = \int_{\vec{t}} x(\vec{t}) e^{-i2\pi \vec{u}^T \vec{t}} d\vec{t} \tag{1}$$

[6] Disambiguation: The term *cone-kernel* is also used in reference to 2D time-frequency representations (Oh and Marks II, 1992; Oh, Marks II, and Atlas, 1994; Zhao, Atlas, and Marks II, 1990) and is not related to the usage of the term here.

[7] An exception would be a gaussian shaped kernel where all tiles are effected by all other tiles at all times. The contribution of shifted kernels far removed will become more and more significant as the kernel expands.

[8] $i = \sqrt{-1}$.

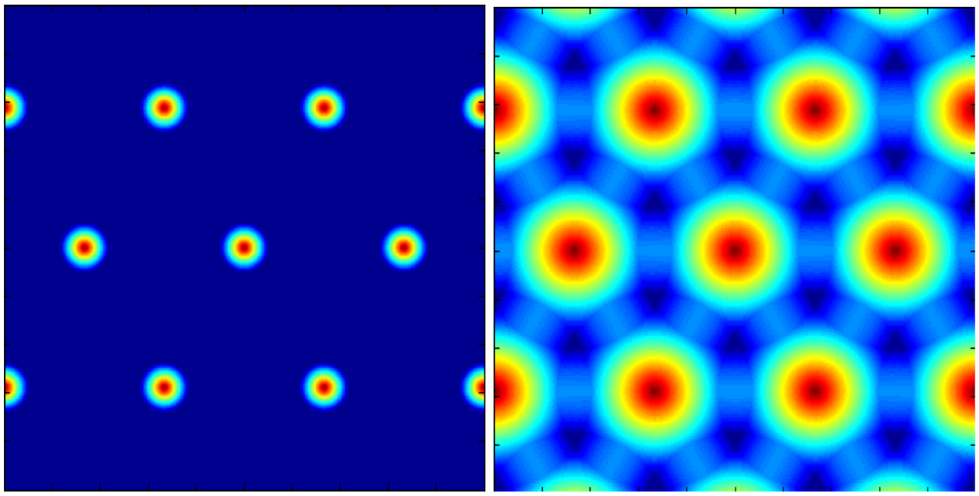

(a) $\sigma = 50$

(b) $\sigma = 200$

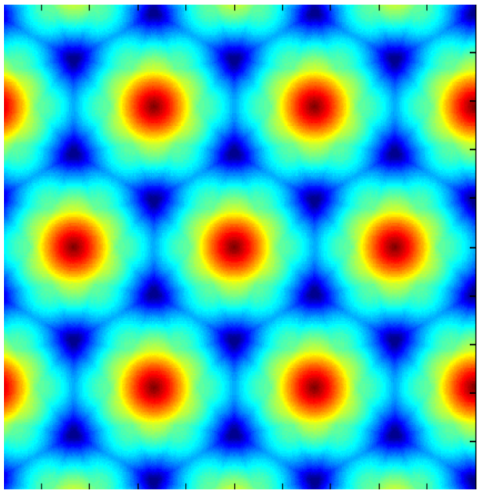

(c) 500

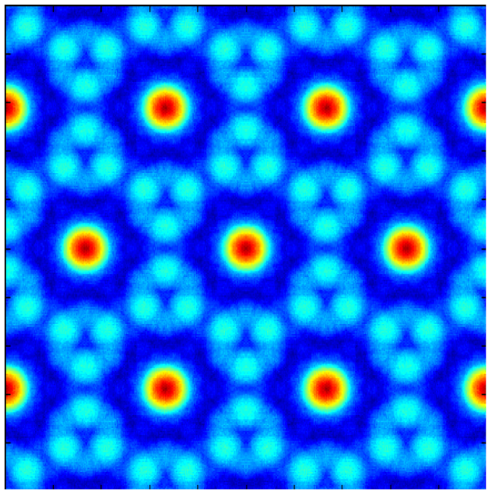

(d) 1000

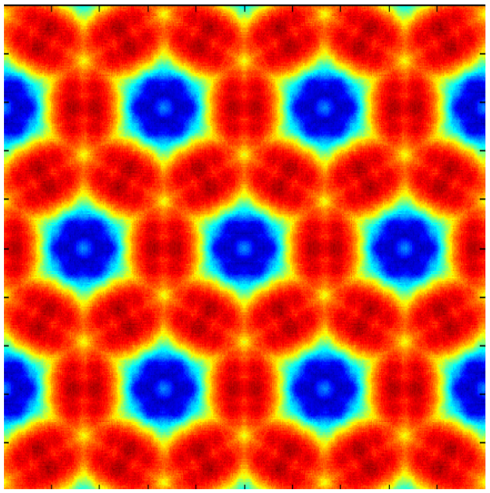

(e) 1500

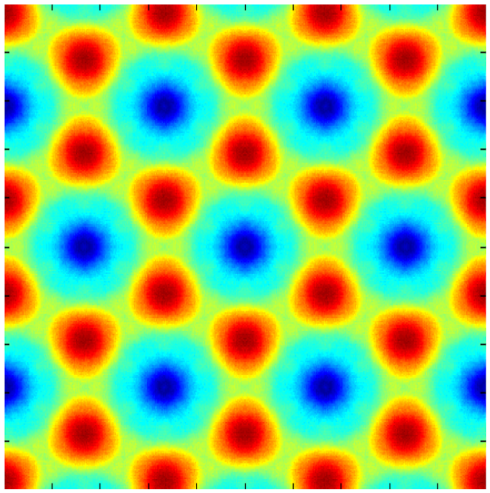

(f) 1750

Figure 14: Heat map plots of the expanding circular cone efflorescent function. The nonoverlapping small cones are seen in (a). (Continued in Figure 15.)

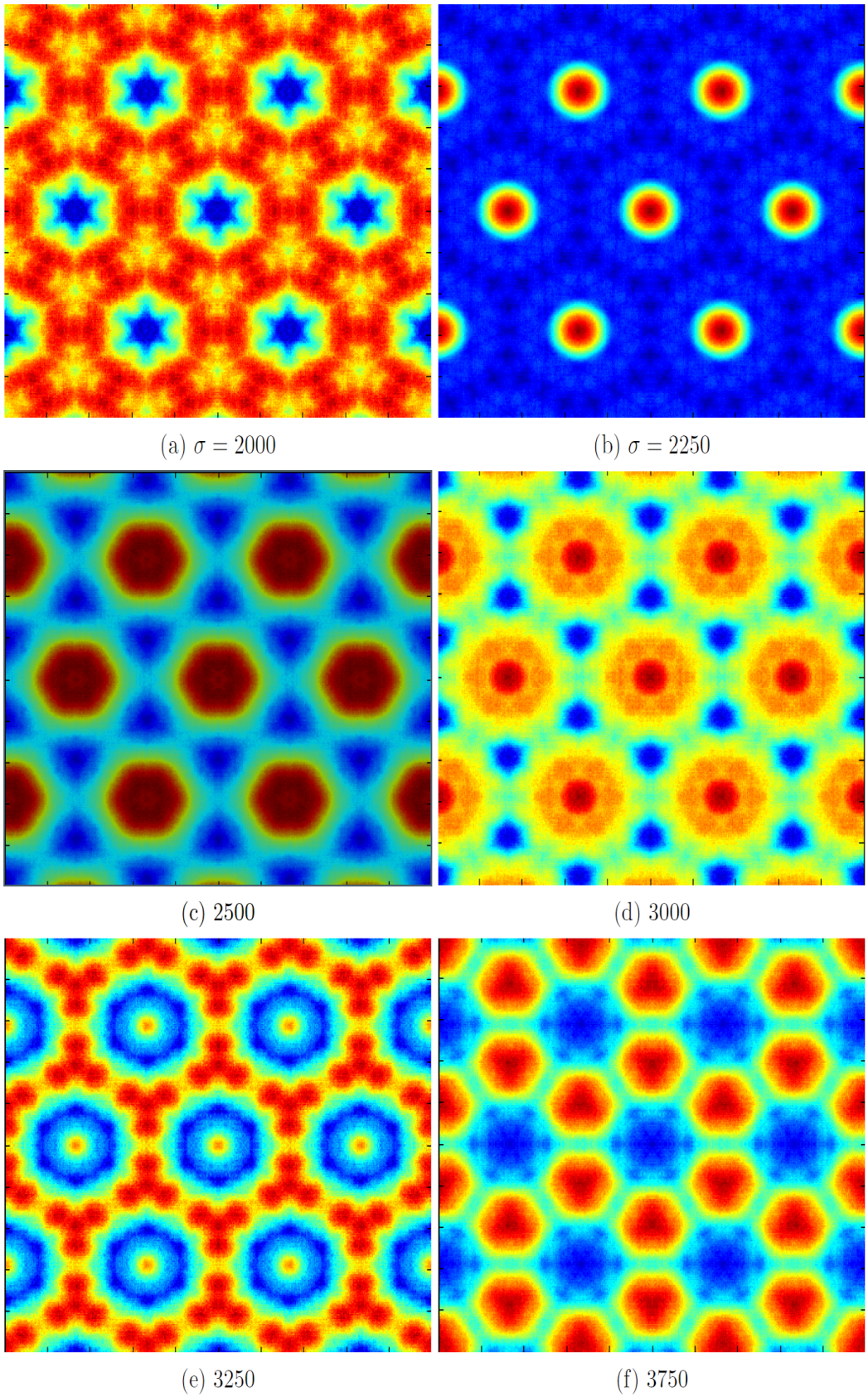

Figure 15: Heat map plots of the expanding circular cone efflorescent function. (Continued from Figure 14.)

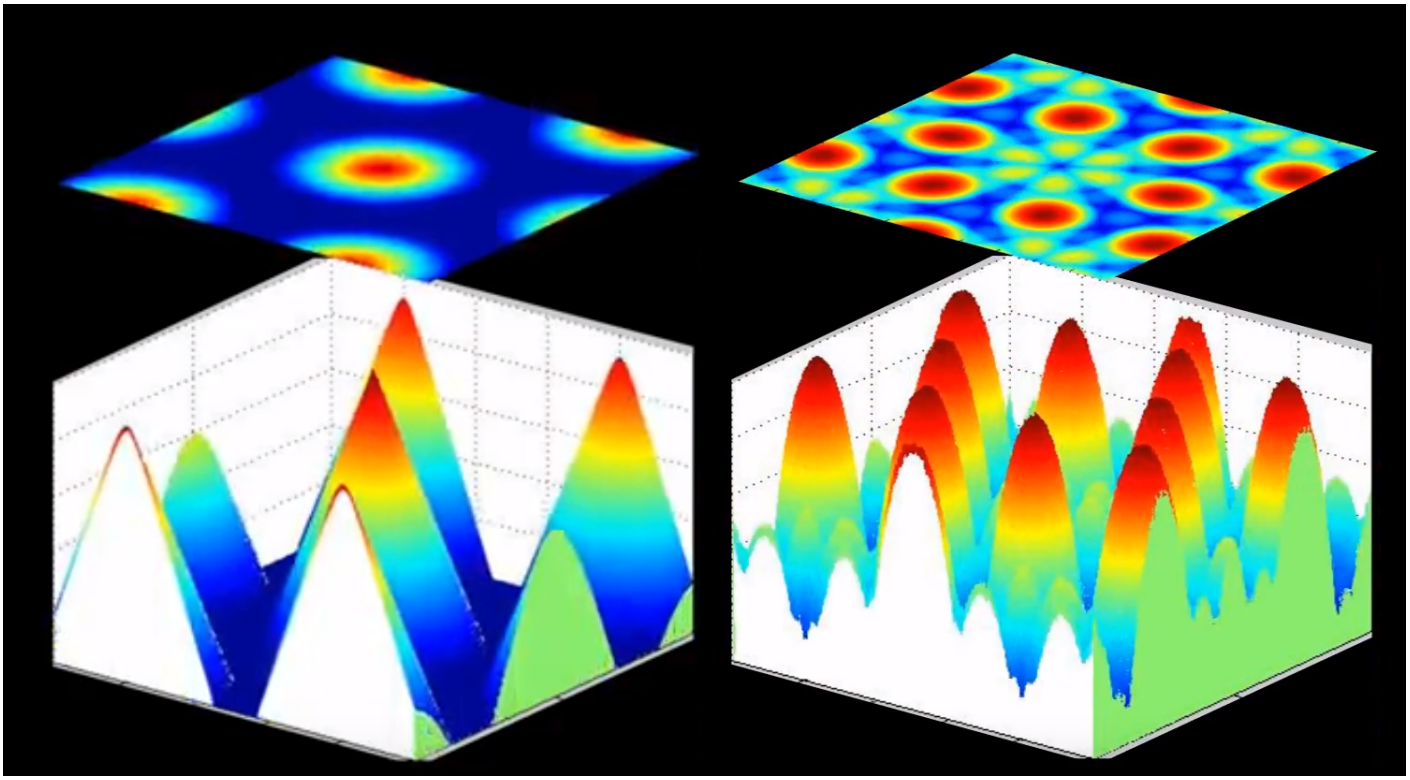

Figure 16: Left: A 2D plot of nonoverlapping replicated circular cones. A perspective projection of the heat map is shown on top. Right: A similar plot made after the expanding circular cones intersect.

where T denotes vector transposition, $\vec{t} = [t_1, t_2]^T$, $\vec{u} = [u_1, u_2]^T$, $d\vec{t} = dt_1 dt_2$ and

$$\int_{\vec{t}} = \int_{t_1} \int_{t_2}.$$

The *signal integral property* (Marks II, 2009) follows immediately from (1) by setting $\vec{u} = \vec{0}$.

$$X(\vec{0}) = \int_{\vec{t}} x(\vec{t}) d\vec{t}. \tag{2}$$

The inverse Fourier transform is

$$x(\vec{t}) = \int_{\vec{u}} X(\vec{u}) e^{i2\pi \vec{u}^T \vec{t}} d\vec{u}.$$

To supply foundation and to establish notation, a concise review of multidimensional Fourier series is appropriate (Dudgeon and Mersereau, 1984; Marks II, 1991; Marks II, 2009). The Fourier series has the following properties (Marks II, 2009):

- Convergence is in the mean if a period of the periodic function satisfies *Dirichlet conditions* criteria.
- Convergence is uniform if the periodically replicated kernel is continuous.
- When there are discontinuities in the kernel, the Fourier series converges to the arithmetic midpoint of the discontinuity.

The examples in this paper are for one and two dimensional periodic functions although the theory can be developed for an arbitrary dimension.

Two dimensional periodicity is dictated by a 2×2 nonsingular periodicity matrix $\mathbf{Q}$ given as

$$\mathbf{Q} = [\vec{q}_1 \vec{q}_2]$$

where $\vec{q}_1$ and $\vec{q}_2$ are *periodicity vectors*. In one dimension, the period of a periodic function is defined by a single scalar which can be viewed as a 1×1 matrix. The scalar entry in the matrix is the one dimensional period, T. In two dimensions, a pair of 2D vectors is required to define periodicity. In M dimensions, M periodicity vectors are required. Each vector is of length M (Dudgeon and Mersereau, 1984; Marks II, 1991; Marks II, 2009),

A 2D example is shown in Figure 17 where maximally packed circles of radius R generate periodicity vectors

$$\vec{q}_1 = \begin{bmatrix} \frac{R}{2} \\ \\ \frac{R}{2\sqrt{3}} \end{bmatrix}; \quad \vec{q}_2 = \begin{bmatrix} -\frac{R}{2} \\ \\ \frac{R}{2\sqrt{3}} \end{bmatrix}.$$

where R is the circle's radius. The corresponding *periodicity matrix* follows as

$$\mathbf{Q} = \frac{R}{2} \begin{bmatrix} 1 & -1 \\ \sqrt{3} & \sqrt{3} \end{bmatrix}. \tag{3}$$

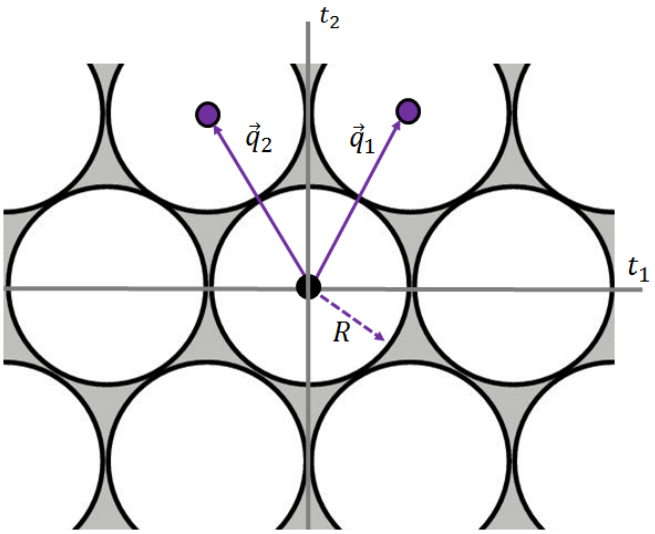

Figure 17: Hexagonal periodicity vectors illustrated for maximally packed circles.

A tile isolates a single period of the periodic function and, when replicated according to the periodicity matrix, fills the space without gaps. For hexagonal periodicity, a corresponding hexagonal tile is shown in Figure 5. For a given periodicity structure, neither $\mathbf{Q}$ or the tile shape is unique. This is illustrated Figure 18 where hexagon and a parallelogram tiles both have the same periodicity vectors.

A tile centered at the origin will be replicated on the (t_1, t_2) plane at the vectors $\vec{q}_1$ and $\vec{q}_2$. The tile will also be replicated at any integer multiple of the periodicity vectors, for example at $\vec{q}_1 + \vec{q}_2$ and $4\vec{q}_1 - 3\vec{q}_2$. Any tile replication on the (t_1, t_2) plane can be represented by the combination $m_1\vec{q}_1 + m_2\vec{q}_2$ where m_1 and m_2 are integers. A more concise expression is

$$m_1\vec{q}_1 + m_2\vec{q}_2 = \mathbf{Q}\vec{m}$$

where $\vec{m}$ is a two dimensional vector of integers.

$$\vec{m} = \begin{bmatrix} m_1 \\ m_2 \end{bmatrix}.$$

The hexagonally shaped tile in Figure 5 has an area of

$$|\det \mathbf{Q}| = \frac{\sqrt{3}\, R^2}{2}. \tag{4}$$

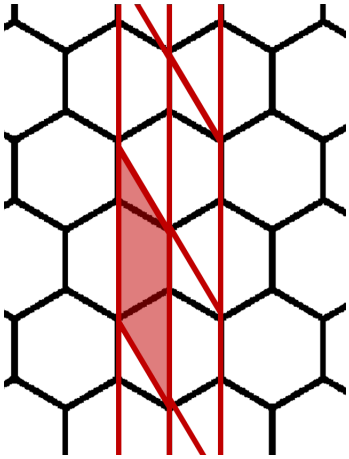

Figure 18: For a given set of periodicity vectors, the choice of tiles is not unique. The periodicity vectors illustrated at the bottom of Figure 17 can also describe the parallelogram tile shown here. (Only two columns of the parallelogram tile are shown here.) In both cases, the area of the tile, $|\det Q|$, is the same (Marks II, 2009).

For a given periodicity structure defined by the periodicity matrix $\mathbf{Q}$, a periodic function with a kernel of $g(\vec{t})$ can be written in a space with coordinates $\vec{t}$ as (Marks II, 2009)

$$z(\vec{t}) = \sum_{\vec{m}} g(\vec{t} - \mathbf{Q}\vec{m}) \tag{5}$$

where the sum is over the set of all integer pairs.

$$\sum_{\vec{m}} = \sum_{m_1=-\infty}^{\infty} \sum_{m_2=-\infty}^{\infty}.$$

Note that

- the kernel is not constrained to be zero outside of a tile and can even extend over the entire $\vec{t}$ plane, and
- many kernels can generate the same periodic function, $z(\vec{t})$.

The corresponding multidimensional Fourier series of the periodic function in (5) is the Fourier series (Marks II, 2009; Papoulis, 1978)[9]

$$z(\vec{t}) = |\det \mathbf{P}| \sum_{\vec{m}} G(\mathbf{P}\vec{m}) \exp\left(i2\pi \vec{t}^T \mathbf{P}\vec{m}\right) \tag{6}$$

[9] To see the periodicity, consider shift of (6) from $z(\vec{t})$ to $z\left(\vec{t} - \mathbf{Q}\vec{k}\right)$ where $\vec{k}$ is an arbitrary vector of integers. If $z\left(\vec{t} - \mathbf{Q}\vec{k}\right) = z(\vec{t})$ for all such shifts. $z(\vec{t})$ is periodic with periodicity matrix $\mathbf{Q}$. From (6),

$$z\left(\vec{t} - \mathbf{Q}\vec{k}\right) = |\det \mathbf{P}| \sum_{\vec{m}} G(\mathbf{P}\vec{m}) \exp\left(i2\pi \left(\vec{t} - \mathbf{Q}\vec{k}\right)^T \mathbf{P}\vec{m}\right).$$

The exponential term here becomes

$$\exp\left(j2\pi \left(\vec{t} - \mathbf{Q}\vec{k}\right)^T \mathbf{P}\vec{m}\right) = \exp\left(i2\pi \vec{t}^T \mathbf{P}\vec{m}\right) \exp\left(-i2\pi \left(\mathbf{Q}\vec{k}\right)^T \mathbf{P}\vec{m}\right).$$

Using (7),

$$\exp\left(-i2\pi \left(\vec{k}^T \mathbf{Q}^T \mathbf{P}\vec{m}\right)\right) = \exp\left(-i2\pi \left(\vec{k}^T \vec{m}\right)\right) = 1$$

so that $z\left(\vec{t} - \mathbf{Q}\vec{k}\right) = z(\vec{t})$.

where $\mathbf{P}$ and $\mathbf{Q}$ are related by an inverse transpose

$$\mathbf{P} = \mathbf{Q}^{-T}, \tag{7}$$

The equivalence of (5) and (6) stems from the Fourier dual of the *Poisson sum formula* (Marks II, 2009; Papoulis, 1978; Papoulis and Pillai, 2002).

$$\sum_{\vec{n}} X(\vec{u} - \mathbf{P}\vec{n}) = |\det \mathbf{Q}| \sum_{\vec{n}} x(\mathbf{Q}\vec{n}) e^{i2\pi \vec{u}^T \mathbf{Q}\vec{n}}$$

4.1 Expanding Kernels

We are able to now describe the expanding kernel periodic function for arbitrary periodicity matrix $\mathbf{Q}$ and kernel $g(\vec{t})$.

Definition 4.1. The *expanding kernel periodic function*, $x_\sigma(\vec{t})$, generated by a *kernel* $g(\vec{t})$ is

$$x_\sigma(\vec{t}) = \sum_{\vec{m}} g\left(\frac{\vec{t} - \mathbf{Q}\vec{m}}{\sigma}\right) \tag{8}$$

As σ increases, the kernel expand.

In both the expanding circular pillbox and expanding circular cone examples, σR is the radius of the circle.

From (6), the corresponding Fourier series of the expanding kernel is

$$x_\sigma(\vec{t}) = |\det \mathbf{P}| \sigma^2 \sum_{\vec{m}} G(\sigma \mathbf{P}\vec{m}) \exp\left(i2\pi \vec{t}^T \mathbf{P}\vec{m}\right). \tag{9}$$

The overlapping expanding kernels can be detrended by evaluating the mean value of the periodic function. The mean value in a Fourier series expansion is the zeroth order Fourier series coefficient. This can be evaluating by integrating over a single tile followed by division by the area of the tile.

The theorem to follow uses the arbitrariness of the choice of tiles when integrating. In one dimension, the period of a periodic function, say T, is arbitrary. We can choose the period to be on the interval $0 \le t < T$ or $-T/2 \le t < T/2$. There is a

similar arbitrariness in the choice of a tile. To illustrate, consider a 2D function with hexagonal replication across a plane. Choosing a tile in this function is like choosing a cookie cutter. As illustrated in Figure 18, a hexagonal cookie cutter can be used. But a hexagon is not the only possible tile. As shown in the figure, a cookie cutter shaped like a parallelogram can also be used as can any cookie cutter that satisfies the periodicity constraints.

Notationally, integrating over area C in the following theorem means integration over any single tile. For additional details, see Marks (Marks II, 2009).

Theorem 4.2. *The mean value of the expanding kernel function, $x_\sigma(\vec{t})$, is*

$$\begin{aligned} \langle x_\sigma \rangle &:= \frac{1}{|\det \mathbf{Q}|} \int_{\vec{t}\in C} x_\sigma(\vec{t})\, d\vec{t} \\ &= \sigma^2 |\det \mathbf{P}| \int_{\vec{t}} g(\vec{t})\, d\vec{t} \qquad (10) \\ &= \sigma^2 |\det \mathbf{P}| G(\vec{0}) \qquad (11) \end{aligned}$$

The region C is any region in the $\vec{t}$ space covering a tile.

As σ increases, the detrended sum of the expanding kernels in the $\vec{t}$ plane approaches a without any interesting structure.

Proof. The expression in (10) for the mean of $x_\sigma(\vec{t})$ follows from the $\vec{m} = \vec{0}$ term in the Fourier series in (9). Equation (11) follows from the integral property (2). □

We can now define the detrended periodic function.

Definition 4.3. The periodic *efflorescent function*, $\zeta_\sigma(\vec{t})$, is the detrended expanding kernel function, *i.e.* $x_\sigma(\vec{t})$ minus its mean.

$$\zeta_\sigma(\vec{t}) = x_\sigma(\vec{t}) - \langle x_\sigma \rangle .$$

The corresponding Fourier series of $\zeta_\sigma(\vec{t})$ is simply the Fourier series of $x_\sigma(\vec{t})$ in (9) with the zeroth order Fourier series coefficient $\vec{m} = \vec{0}$ term removed.[10]

$$\zeta_\sigma(\vec{t}) = |\det \mathbf{P}| \sigma^2 \sum_{\vec{m}\neq\vec{0}} G(\sigma \mathbf{P}\vec{m}) \exp\left(i 2\pi \vec{t}^T \mathbf{P}\vec{m}\right). \qquad (12)$$

From this expression, we see the Fourier series coefficients for the efflorescent function are

$$c_\sigma[\vec{m}] = \begin{cases} |\det \mathbf{P}| \sigma^2 G(\sigma \mathbf{P}\vec{m}) & ; \quad \vec{m} \neq \vec{0} \\ 0 & ; \quad \vec{m} \neq \vec{0} \end{cases} \qquad (13)$$

[10] By $\vec{0}$, we mean a vector whose only elements are zero.

4.2 Convergence

The periodic efflorescent function can most interestingly generate a never repeating pattern of fascinating shapes. This does not happen when, as a function of expansion, the efflorescent function reaches a limit cycle or fixed point. We now examine when this happens.

Asymptotic Convergence of the Efflorescent Function to Zero

We first establish when the efflorescent function expanding kernel approaches zero.

First define the *Kronecker delta* as

$$\delta[\vec{m}] := \begin{cases} 1 & ; \quad \vec{m} = \vec{0} \\ 0 & ; \quad \vec{m} \neq \vec{0} \end{cases}$$

Theorem 4.4. Sufficient condition for converging to the mean. *Let $M = 2$.*[11] *If*

$$\sigma^M G(\sigma \mathbf{P}\vec{m}) \underset{\sigma\to\infty}{\longrightarrow} \sigma^M G(\vec{0}) \delta[\vec{m}] \qquad (14)$$

then $x_\sigma(\vec{t})$ converges to its mean.

$$x_\sigma(\vec{t}) \underset{\sigma\to\infty}{\longrightarrow} \langle x_\sigma \rangle .$$

As a consequence

$$\zeta_\sigma(\vec{t}) \underset{\sigma\to\infty}{\longrightarrow} 0.$$

In other words, as the kernels continue to expand, the efflorescent function approaches the very uninteresting result of zero over the entire (t_1, t_2) plane.

Proof. As $\sigma \to \infty$, all terms $\sigma^M G(\sigma \mathbf{P}\vec{m})$ in (9) tend to zero when (14) is true except when $\vec{m} = \vec{0}$. Then (9) becomes

$$x_\sigma(\vec{t}) \underset{\sigma\to\infty}{\longrightarrow} \sigma^M |\det \mathbf{P}| G(\vec{0}) = \langle x_\sigma \rangle$$

□

A sufficient smoothness criterion Convergence of an expanding efflorescent function to zero is assured when the kernel adheres to smoothness and integrability properties.

[11] The theorems given are applicable in any dimension M. We have concentrated on 2D so will set $M = 2$ to avoid confusion. This also applies to Theorem 4.5.

Theorem 4.5. Convergence to the mean: *The following theorem applies to M dimensions. For the examples herein, $M = 2$. The M dimensional function, $x_\sigma(\vec{t})$, converges to its mean if its kernel, $g(\vec{t})$, obeys the following property.*[12]

$$\int_{\vec{t}} \left| \left(\prod_{k=1}^{M} \frac{\partial^{i_k}}{\partial t_k^{i_k}} \right) g(\vec{t}) \right| d\vec{t} = A < \infty \tag{15}$$

where the nonnegative integers $\{i_k | 1 \le k \le M\}$ obey

$$\sum_{k=1}^{M} i_k > M \tag{16}$$

The choice of $\vec{i} = [i_1 \; i_2 \; i_3 \; \cdots \; i_M]^T$ is arbitrary so long as (15) and (16) are satisfied.

The proof is given in Appendix 6.1.

Corollary 4.6. *For $M = 1$, Theorem 4.5 says the efflorescent function will converge to zero if*

$$\int_t \left| \frac{d^2}{dt^2} g(t) \right| dt = A < \infty$$

Example 4.7. Consider the two dimensional kernel

$$g(\vec{t}) = \Pi(t_1) e^{-t_2^2},$$

where the *rectangle function* is

$$\Pi(t) := \begin{cases} 1 & ; \quad |t| \le \frac{1}{2} \\ 0 & ; \quad |t| > \frac{1}{2}. \end{cases} \tag{17}$$

Then (WolframAlpha.com, 2020)

$$\begin{aligned} \int_{\vec{t}} \left| \frac{\partial^3}{\partial t_2^3} g(\vec{t}) \right| d\vec{t} &= \int_{t_1=-\infty}^{\infty} \Pi(t_1) dt_1 \int_{t_2=-\infty}^{\infty} \left| \frac{d^3}{dt_2^3} e^{-t_2^2} \right| dt_2 \\ &= \\ &= 4\left(1 + 4e^{-3/2}\right) = A < \infty \end{aligned}$$

and $i_1 + i_2 = 0 + 3 > M = 2$. The criteria in Theorem 4.5 are met and asymptotic convergence of the efflorescent function to zero is assured.

Asymptotic Convergence To a Fixed Function

As the following example shows, the efflorescent function can converge to a fixed function of $\vec{t}$ as scaling increases.

Example 4.8. Consider the one dimensional kernel

$$g(t) = e^{-t} \mu(t) \tag{18}$$

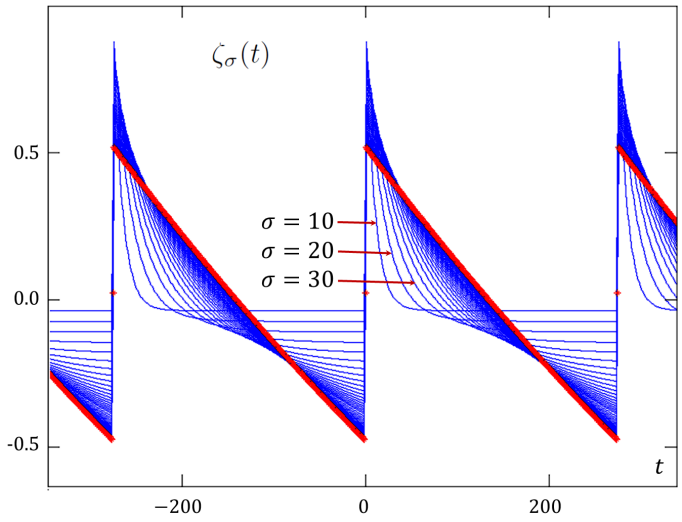

Figure 19: Using the exponential decay kernel in (18) results in the $\zeta_\sigma(t)$'s shown. As $\sigma \to \infty$, the function approaches the sawtooth shown by the thick red line given by (19). (For this plot, $T = 275$.)

where $\mu(t)$ is the Heaviside step function.[13] Then $\zeta_\sigma(\vec{t})$ converges in steady state to the solid red sawtooth waveform shown in Figure 19.

$$\lim_{\sigma \to \infty} \zeta_\sigma(t) = \frac{1}{2} - \frac{t}{T}; \; 0 < t < T \tag{19}$$

A proof is given in Appendix 6.2.

Asymptotic Limit Cycle Periodicity in σ

Efflorescent functions can be asymptotically periodic as a function of the expansion scaling variable σ.

Theorem 4.9. *Using the scalar periodicity matrix $\mathbf{Q} = T$, the one dimensional kernel*

$$g(t) = \Pi(t)$$

results in a efflorescent function periodic in σ with a period of $T_\sigma = 2T$.

Proof. The one dimensional Fourier series expression for the

[12] For $M = 5$ and $\vec{i} = [4 \; 0 \; 1]^T$, for example,

$$\left(\prod_{k=1}^{M} \frac{\partial^{i_k}}{\partial t_k^{i_k}} \right) g(\vec{t}) = \frac{\partial^5}{\partial t_1^4 \partial t_3} g(\vec{t}).$$

[13] Equal to one for positive argument and zero otherwise.

efflorescent function is

$$\zeta_\sigma(t) = \frac{\sigma}{T} \sum_{m \neq 0} \operatorname{sinc}\left(\frac{\sigma m}{T}\right) e^{i2\pi m t/T}. \tag{20}$$

where

$$\operatorname{sinc}(u) := \frac{\sin(\pi u)}{\pi u}$$

is the one dimensional Fourier transform of $\Pi(t)$. For $m \neq 0$, the mth Fourier series coefficient is

$$\begin{aligned} c_\sigma[m] = \sigma G\left(\frac{\sigma m}{T}\right) &= \frac{\sigma}{T} \operatorname{sinc}\left(\frac{\sigma m}{T}\right) \\ &= \\ &= \frac{1}{T} \frac{\sin\left(\frac{\pi m \sigma}{T}\right)}{\pi m} \end{aligned}$$

Because of the sin term, $c_\sigma[m]$ is periodic with respect to σ with period $2T$.

$$c_{\sigma+2T}[m] = c_\sigma[m]$$

Since all of the Fourier series coefficients in (20) are periodic with period $2T$, we conclude that

$$\zeta_{\sigma+2T}(t) = \zeta_\sigma(t).$$

and the efflorescent function oscillates as a function of σ. □

The periodicity of $\zeta_\sigma(t)$ is illustrated in Figure 20. The function is bounded by $|\zeta_\sigma(t)| \leq 1$ and is plotted over a single period. The Figure begins with an all zero function marked with the number 0. σ increases a bit. For the function marked 1, there is now a short positive pulse and the remainder of the function is zero. Since $\langle \zeta_\sigma \rangle = 0$, all of the functions shown have zero area. The pulse at the origin begins to spread as σ increases as is seen in the functions marked 2 through 7. Then, at 8, the function returns to being identically zero. The second phase is shown in Figure 20b. We begin with the zero function marked 8 in Figure 20a which is also marked 8 in Figure 20b. σ increases a bit. The function marked 9 is a short negative pulse. As σ increases, the negative pulse widens as is seen in the functions marked 9 through 15. Function 16 is identically zero and is the same as the function marked 0 in Figure 20a. One period is complete and, as σ increases, the next identical period begins.

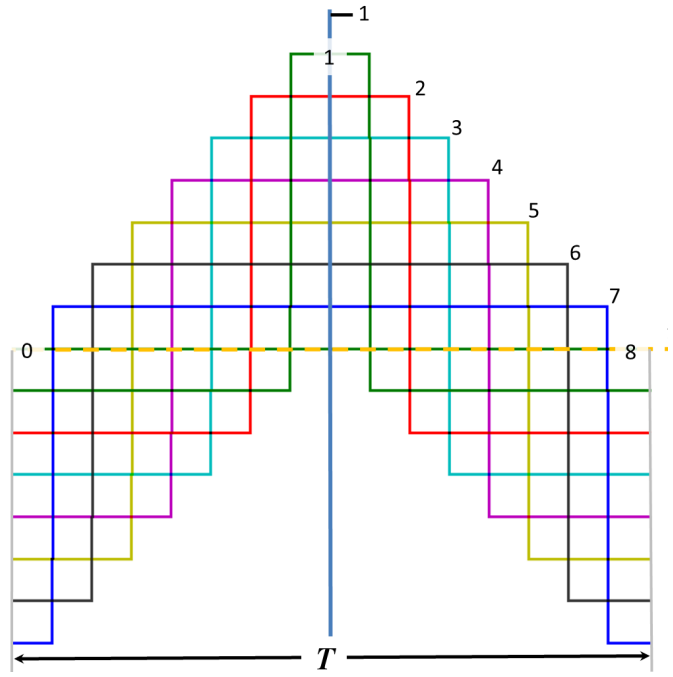

(a) The first part of the periodicity in σ.

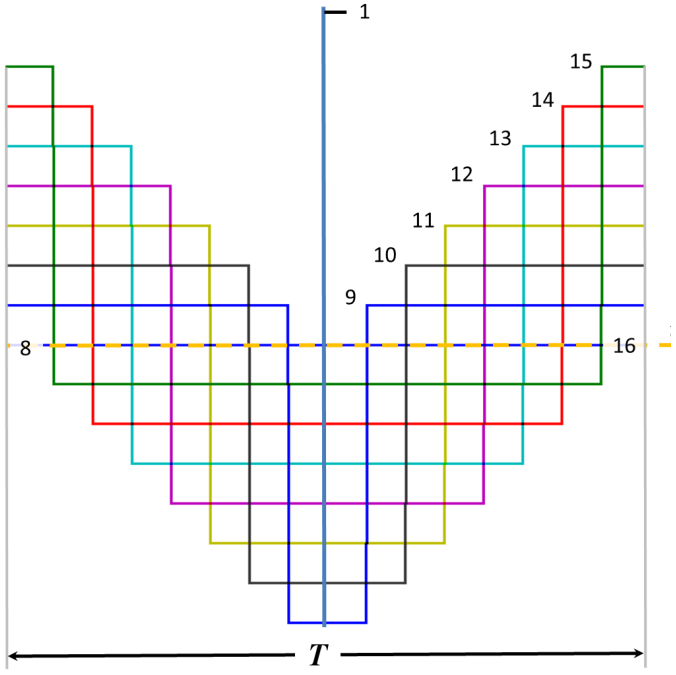

(b) The second part.

Figure 20: The periodicity in σ of $\zeta_\sigma(t)$ for expanding rectangular kernels in (20). The period in σ is $2T$. The function $\zeta_\sigma(t)$ is also periodic in t with period T.

4.3 Efflorescent Examples

The most interesting of efflorescent functions are those that have no fixed asymptotic convergence properties. In two dimensions, such efflorescent functions continually bloom in a nonrepeating manner. The reader is encouraged to view the online videos (Nybal, 2014d; Nybal, 2014c; Nybal, 2014b; Nybal, 2014a) (especially the expanding pillbox cone and circular

cone videos) to fully appreciate this emergence. Screen shots for expanding circle and cone shaped kernels are shown in Figures 3, 14 and 15. We now analyze properties of these two kernel types.

We find useful the radial measures

$$r = \|\vec{t}\| \text{ and } \rho = \|\vec{u}\|$$

where

$$\|\vec{t}\| = \sqrt{t_1^2 + t_2^2}. \tag{21}$$

When the variable $r = r(t_1, t_2)$ is used in a two dimensional expression, we assume it to be a two dimensional function of t_1 and t_2 as expressed here. Doing so avoids writing out the square root expression in (21) at each usage. The variable $\rho = \rho(u_1, u_2)$ can similarly be interpreted as a function of u_1 and u_2.

Expanding Pillbox Circle Example

The expanding circles example is a special case of (8) for $M = 2$ dimensions where the kernel $g(\vec{t})$ is one inside a circle of unit radius and is otherwise zero.[14]

$$g(\vec{t}) = \Pi\left(\frac{r}{2}\right). \tag{22}$$

Then $G(\vec{0})$ is simply the area of a unit radius circle. From the signal integral property in (2).

$$G(\vec{0}) = \int_{\vec{t}} \Pi\left(\frac{r}{2}\right) d\vec{t} = \pi.$$

For expanding circles, the expanding kernel function is

$$x_\sigma\left(\vec{t}\right) = \sum_{\vec{m}} \Pi\left(\frac{\|\vec{t} - \mathbf{Q}\vec{m}\|}{2\sigma}\right)$$

so that $g\left(\frac{\vec{t}-\mathbf{Q}\vec{m}}{\sigma}\right)$ in the $\vec{m}$th tile is a circle of radius σ centered at $\mathbf{Q}\vec{m}$.

The 2D Fourier transform of a unit radius circle in (22) is (Marks II, 2009)

$$G\left(\vec{u}\right) = \frac{J_1(2\pi\rho)}{2\rho}$$

where $J_1(\cdot)$ is a first order Bessel function of the first kind. Asymptotically (Abramowitz and Stegun, 1972)

$$\frac{J_1(2\pi\rho)}{2\rho} \underset{\rho\to\infty}{\longrightarrow} \frac{\rho^{-3/2}}{2\pi}\cos\left(2\pi\rho - \frac{3}{4}\pi\right) \tag{23}$$

so that, for $\vec{m} \neq \vec{0}$,

$$\begin{aligned}\sigma^2 G(\sigma\mathbf{P}\vec{m}) &= \sigma^2 \frac{J_1(2\pi\sigma\|\mathbf{P}\vec{m}\|)}{2\sigma\|\mathbf{P}\vec{m}\|} \\ &\underset{\sigma\to\infty}{\longrightarrow} \frac{1}{2\pi}\sqrt{\frac{\sigma}{\|\mathbf{P}\vec{m}\|^3}}\cos\left(2\pi\sigma\|\mathbf{P}\vec{m}\| - \frac{3}{4}\pi\right)\end{aligned}$$

The sufficient condition of Theorem 4.4 for convergence of the efflorescent function to zero is therefore not met.

Pillbox Expansion on a Hexagonal Grid We have yet to specify a periodicity for the expanding circles. Assume the circle centers are spaced hexagonally in accordance with the periodicity matrix in (3). From (4) we see that

$$|\det \mathbf{P}| = \frac{1}{|\det \mathbf{Q}|} = \frac{2}{\sqrt{3}R^2}. \tag{24}$$

The expanding kernel function's mean, from (10), is therefore

$$\langle x_\sigma \rangle = \sigma^2\left(\frac{2}{\sqrt{3}R^2}\right)\pi = \frac{2\pi\sigma^2}{\sqrt{3}R^2}$$

Screen shots for the efflorescent function is shown in Figure 3 from the video available online (Nybal, 2014d).

Expanding Circular Cones

Set the two dimensional kernel to a circular cone of unit height.

$$g\left(\vec{t}\right) = (1 - r)\Pi\left(\frac{r}{2}\right)$$

For circularly symmetric functions, the 2D Fourier transform becomes the Hankel transform (Marks II, 2009) so that (WolframAlpha.com, 2020) becomes

$$\begin{aligned}G\left(\vec{u}\right) &= 2\pi\int_0^1 r(1-r)J_0(2\pi r\rho)dr \\ &= \frac{H_0(2\pi\rho)J_1(2\pi\rho) - H_1(2\pi\rho)J_0(2\pi\rho)}{4\rho^2}.\end{aligned} \tag{25}$$

where $H_n(\cdot)$ are *Struve functions* (Weisstein, 2020) and $J_n(\cdot)$ are Bessel functions of the first kind. In Appendix 6.3, we show that

$$\sigma^2 G(\sigma\mathbf{P}\vec{m}) \underset{\sigma\to\infty}{\longrightarrow} -\frac{2}{\pi^2}\sqrt{\frac{\sigma^3}{\|\mathbf{P}\vec{m}\|}}\cos\left(2\pi\sigma\|\mathbf{P}\vec{m}\| - \frac{\pi}{4}\right). \tag{26}$$

As is the case with the expanding circles, the condition of Theorem 4.4 for convergence to the mean for the expanding cones is therefore not met. For any fixed $\mathbf{P}$ and $\vec{m} \neq \vec{0}$, the limit does not approach zero as σ increases without bound.

[14] Specifically, from the definition of $\Pi(\cdot)$ in (17), $g(\vec{t}) = \Pi(r/2)$ is one for $\frac{r}{2} < \frac{1}{2}$. This is equivalent to $r = \|\vec{t}\| = \sqrt{t_1^2 + t_2^2} < 1$ which defines a circle of unit radius.

Circular Cone Expansion on a Hexagonal Grid Assume the cone centers are spaced hexagonally in accordance with the periodicity matrix in (3). Thus we can use (24). Since $J_0(0) = 1$, the volume of a cone with a unit circle base and unit height is, from (25),

$$G(\vec{0}) = 2\pi \int_0^1 r(1-r)dr = \frac{\pi}{3}.$$

The expanding kernel function's mean, from (10), is then

$$\langle x_\sigma \rangle = \sigma^2 \left(\frac{2}{\sqrt{3}R^2} \right) \frac{\pi}{3} = \frac{2\sqrt{3}\pi\sigma^2}{R^2}.$$

As was the case for the circular pillbox, the limit does not approach zero as σ increases without bound. Screen shots for the cone's efflorescent function are shown in Figures 14 and 15 from the video available online (Nybal, 2014c).

5 Conclusions

We have introduced the idea of periodic expanding kernel and efflorescent functions and have shown they can display widely variant behaviors dependent on the kernel and the underlying periodicity. Examples are given of efflorescent functions that converge to zero, converge to a nonconstant fixed point and oscillate. When the efflorescent functions fluctuate without repeating, patterns reminiscent of continual blooming can emerge. Special occurrences for a circular pillbox kefor of the three petal geometry representing Christianity's trinity and the flower-of-life. All emergent patterns are periodic and can be used for artful tiling.

6 Appendices

6.1 Proof of Theorem 4.5: Convergence to the mean

The derivative theorem of Fourier analysis indicates

$$\left(\prod_{k=1}^{M} \frac{\partial^{i_k}}{\partial t_k^{i_k}} \right) g\left(\vec{t}\right)$$

has a Fourier transform of

$$\left(\prod_{k=1}^{M} (j2\pi u_k)^{i_k} \right) G\left(\vec{u}\right)$$

Thus

$$G\left(\vec{u}\right) = \frac{\int_{\vec{t}} \left[\left(\prod_{k=1}^{M} \frac{\partial^{i_k}}{\partial t_k^{i_k}} \right) g\left(\vec{t}\right) \right] e^{-i2\pi \vec{t}^T \vec{u}} d\vec{t}}{\prod_{k=1}^{M} (j2\pi u_k)^{i_k}}.$$

and

$$\begin{aligned} \left|G\left(\vec{u}\right)\right| &= \frac{\left| \int_{\vec{t}} \left[\left(\prod_{k=1}^{M} \frac{\partial^{i_k}}{\partial t_k^{i_k}} \right) g\left(\vec{t}\right) \right] e^{-j2\pi \vec{t}^T \vec{u}} d\vec{t} \right|}{(2\pi)^{\tilde{M}} \prod_{k=1}^{M} |u|_k^{i_k}} \\ &= \\ &\leq \frac{\int_{\vec{t}} \left| \left(\prod_{k=1}^{M} \frac{\partial^{i_k}}{\partial t_k^{i_k}} \right) g\left(\vec{t}\right) \right| d\vec{t}}{(2\pi)^{\tilde{M}} \prod_{k=1}^{M} |u|_k^{i_k}} \\ &= \\ &= \frac{A}{(2\pi)^{\tilde{M}} \prod_{k=1}^{M} |u|_k^{i_k}} \end{aligned}$$

where

$$\tilde{M} = \sum_{k=1}^{M} i_k. \tag{27}$$

Continuing

$$\sigma^M \left|G(\sigma\vec{u})\right| \leq \frac{A\sigma^M}{(2\pi\sigma)^{\tilde{M}} \prod_{k=1}^{M} |u|_k^{i_k}}$$

and

$$\sigma^M \left|G(\sigma\mathbf{P}\vec{m})\right| \leq \frac{A\sigma^{M-\tilde{M}}}{(2\pi)^{\tilde{M}} \prod_{k=1}^{M} |(\mathbf{P})_k \vec{m}|^{i_k}}.$$

With all other parameters fixed, this expression tends to zero for increasing σ when

$$M - \tilde{M} < 0$$

or, using (27),

$$\sum_{k=1}^{M} i_k > M$$

6.2 Proof of Theorem 4.8: Convergence to a fixed periodic function

Applying the exponential kernel in (18) to (8) for scalar $\mathbf{Q} = T$ gives

$$\begin{aligned} x_\sigma(t) &= \sum_{m=-\infty}^{\infty} \exp\left(-\frac{t-mT}{\sigma} \right) \mu(t-mT) \\ &= e^{-t/\sigma} \sum_{m=-\infty}^{\infty} e^{mT/\sigma} \mu(t-mT) \end{aligned}$$

Over the period $0 \le t < T$,

$$x_\sigma(t) = e^{-t/\sigma} \sum_{m=-\infty}^{0} e^{mT/\sigma}.$$

Using a geometric series

$$x_\sigma(t) = \frac{e^{-t/\sigma}}{1 - e^{-T/\sigma}}$$

and

$$\zeta_\sigma(t) = x_\sigma(t) - \frac{\sigma}{T}.$$

Express the exponentials as a truncated Taylor series.

$$\zeta_\sigma(t) = \frac{1 - \frac{t}{\sigma} + \frac{t^2}{2\sigma^2}}{\frac{T}{\sigma} - \frac{T^2}{2\sigma^2}} - \frac{\sigma}{T}.$$

After some manipulation

$$\begin{aligned} \zeta_\sigma(t) &\underset{\sigma\to\infty}{\longrightarrow} \frac{\sigma\left(t - \frac{T}{2}\right) + \frac{t^2}{2}}{T\left(\sigma - \frac{T}{2}\right)} \\ &\underset{\sigma\to\infty}{\longrightarrow} \frac{1}{2} - \frac{t}{T} \end{aligned}$$

which is the desired result in (19).

6.3 Proof of (26): Cone convergence

The Struve functions used in (26) can be defined by their Taylor series (Weisstein, 2020)

$$H_0(z) = \frac{2}{\pi} \sum_{k=0}^{\infty} \frac{(-1)^k z^{2k+1}}{[(2k+1)!!]^2}$$

and

$$H_1(z) = \frac{2}{\pi} \sum_{k=0}^{\infty} \frac{(-1)^{k+1} z^{2k}}{(2k-1)!!(2k+1)!!}.$$

They have the following asymptotic behavior (Wolfram Research, 2020b)

$$H_0(z) \underset{|z|\to\infty}{\longrightarrow} \sqrt{\frac{2}{\pi z}} \sin\left(z - \frac{\pi}{4}\right)\left(1 + O\left(\frac{1}{z^2}\right)\right)$$

and

$$H_1(z) \underset{|z|\to\infty}{\longrightarrow} \frac{2}{\pi}\left(1 + O\left(\frac{1}{z^2}\right)\right).$$

Likewise, the Bessel function has the asymptotic behavior (Wolfram Research, 2020a)

$$J_0(z) \underset{|z|\to\infty}{\longrightarrow} \sqrt{\frac{2}{\pi z}} \cos\left(z - \frac{\pi}{4}\right)\left(1 + O\left(\frac{1}{z^2}\right)\right)$$

and

$$J_1(z) \underset{|z|\to\infty}{\longrightarrow} \sqrt{\frac{2}{\pi z}} \cos\left(z - \frac{3\pi}{4}\right)\left(1 + O\left(\frac{1}{z^2}\right)\right)$$

In light of these behaviors, inspection of (26) reveals the $H_1(z)J_0(z)$ term asymptotically dominates the $H_0(z)J_1(z)$ term and

$$H_1(2\pi\rho)J_0(2\pi\rho) \underset{\rho\to\infty}{\longrightarrow} \frac{2}{\pi^2}\rho^{-\frac{1}{2}} \cos\left(2\pi\rho - \frac{\pi}{4}\right).$$

Thus

$$\sigma^2 G(\sigma\vec{u}) \underset{\sigma\to\infty}{\longrightarrow} -\frac{2}{\pi^2}\sqrt{\frac{\sigma^3}{\rho}} \cos\left(2\pi\sigma\rho - \frac{\pi}{4}\right)$$

from which (26) follows.

References

Abramowitz, M and I A Stegun, eds. (1972). *Handbook of Mathematical Functions: With Formulas, Graphs, and Mathematical Tables*. Vol. 55. Courier Dover Publications.

Adamantios (2013). Available under the Creative Commons Attribution-Share Alike 3.0 Unported license. URL: `https://commons.wikimedia.org/wiki/File:China-beijing-forbidden-city-P1000157-detail.jpg`.

da Vinci, Leonardo (1478). URL: `https://commons.wikimedia.org/wiki/File:Leonardo_da_Vinci_-_Codex_Atlanticus_folio_307v.jpg`.

Dudgeon, D E and R M Mersereau (1984). *Multidimensional Digital Signal Processing*. Vol. 1. Prentice-Hall Signal Processing Series. Englewood Cliffs: Prentice-Hall.

Feldkamp, L A, L C Davis, and J W Kress (1984). "Practical cone-beam algorithm". In: *JOSA* 6, pp. 612–619.

Filipovic, D S, J L Volakis, and L S Andersen (1999). "Efficient modeling and analysis of infinite periodic antenna arrays by tetrahedral finite elements". In: *Antennas and Propagation Society International Symposium*. Vol. 4. IEEE, pp. 2504–2507.

Flowers, Ray (2006). Available under the Creative Commons Attribution-Share Alike 3.0 Unported license. URL: `https://commons.wikimedia.org/wiki/File:Temple-of-Osiris_Flower-of-Life_02.jpg`.

Goussetis, G, A P Feresidis, and J C Vardaxoglou (2006). "Tailoring the AMC and EBG characteristics of periodic metallic arrays printed on grounded dielectric substrate". In: *IEEE Transactions on Antennas and Propagation* 54.1, pp. 82–89.

Hill, M O and H G Gauch (1980). "Detrended correspondence analysis: an improved ordination technique". In: *Classification and Ordination*, pp. 47–58.

Ishimaru, A et al. (1985). "Finite periodic structure approach to large scanning array problems". In: *IEEE Transactions on Antennas and Propagation* 33.11, pp. 1213–1220.

Kantelhardt, J W et al. (2002). "Multifractal detrended fluctuation analysis of nonstationary time series". In: *Physica A: Statistical Mechanics and its Applications* 316.1–4, pp. 87–114.

Manninen, Marko (2011). Available under the Creative Commons Attribution-Share Alike 4.0 International license. URL: https://commons.wikimedia.org/wiki/File:Floor_decoration_from_the_palace_of_King_Ashurbanipal.jpg.

Markov, G T and A F Chaplin (1983). *The Excitation of Electromagnetic Waves*. 2nd revised and enlarged edition. Moscow Izdatel Radio Sviaz.

Marks II, R J (1991). *Introduction to Shannon Sampling and Interpolation Theory*. Springer-Verlag.

Marks II, R J (2009). *Handbook of Fourier Analysis and Its Applications*. Oxford University Press.

Marks II, R J (2019). "Subtile Sampling Below the Nyquist Density Using Transposed and Rotated Signals". In: *JOSA A* 36.8, pp. 1322–1332.

Melchizedek, D (1999). *The Ancient Secret of the Flower of Life*. Vol. 1. Light Technology Publishing.

Mic, P (2012). "'Flower of Life' Drawings by Leonardo da Vinci". In: *The Monkey Buddha* October 15.

Miryam, I (2015). *Flower of life ephesos square*. Available under the Creative Commons Attribution-Share Alike 4.0 International license. URL: https://commons.wikimedia.org/wiki/File:Flower_of_life_ephesos_square.jpg.

National Geographic (2010). *Crop Ciscle Mystery*. URL: https://youtu.be/3pDmrWwPhpg.

Nguyen, M (2007). *Cup Idalion Louvre*. URL: https://commons.wikimedia.org/wiki/File:Cup_Idalion_Louvre_N3454.jpg.

Nybal, I (2014a). *2,866 Expanding Psychedelic Diamond Hexes*. URL: http://youtu.be/VO-pWA1BSmg.

Nybal, I (2014b). *Boring Expanding Rectangular Rectangles*. URL: http://youtu.be/zojd8hC6d8E.

Nybal, I (2014c). *Exploding Cones on a Hex Grid*. URL: http://youtu.be/sT3ccZgLmnY.

Nybal, I (2014d). *Ten Thousand Expanding Psychedelic Circle Hexes*. URL: http://youtu.be/bXoP5F0s33c.

Oh, S and R J Marks II (1992). "Some properties of the generalized time frequency representation with cone shaped kernels". In: *IEEE Transactions on Signal Processing* 40.7, pp. 1735–1745. URL: http://robertmarks.org/REPRINTS/1992-07_SomePropertiesOfTheGeneralized.pdf.

Oh, S, R J Marks II, and L E Atlas (1994). "Kernel synthesis for generalized time-frequency distributions using the method of alternating projections onto convex sets". In: *IEEE Transactions on Signal Processing* 42.7, pp. 1653–1661. URL: http://robertmarks.org/REPRINTS/1994-07_KernelSythesisForGeneralized.pdf.

Papoulis, A (1978). *Signal analysis*. Vol. 191. New York: McGraw-Hill.

Papoulis, A and S U Pillai (2002). *Probability, Random Variables, and Stochastic Processes*. Tata McGraw-Hill Education.

Scarfe, W C (2018). "Cone beam computed tomography". In: *White and Pharoah's Oral Radiology: Principles and Interpretation*, p. 150.

Sung, Y et al. (2008). "Sensor configuration and activation for field detection in large sensor arrays". In: *IEEE Transactions on Signal Processing* 56.2, pp. 447–463.

Weisstein, E (2020). "Struve Function". In: *Wolfram Math World*. URL: http://mathworld.wolfram.com/StruveFunction.html.

Wikipedia (2020a). *Heat Map*. URL: https://en.wikipedia.org/wiki/Heat_map.

Wikipedia (2020b). *Single penny image*. URL: https://en.wikipedia.org/wiki/Penny_(United_States_coin).

Wikipedia (2020c). *Triquetra*. URL: https://en.wikipedia.org/wiki/Triquetra.

Wolfram Research (2020a). "Bessel Functions of the First Kind". In: *Wolfram Functions Site*. URL: http://functions.wolfram.com/Bessel-TypeFunctions/BesselJ/06/02/03/01/.

Wolfram Research (2020b). "StruveH". In: *Wolfram Functions Site*.

WolframAlpha.com (2020). *Integration solved using Wolfram Alpha*.

Zhao, Y, L E Atlas, and R J Marks II (1990). "The use of cone-shaped kernels for generalized time-frequency representations of nonstationary signals". In: *IEEE Transactions on Acoustics, Speech and Signal Processing* 38, pp. 1084–1091. URL: http://robertmarks.org/REPRINTS/1990-07_TheUseOfCone.pdf.